Fire and Materials

WILEY

RESEARCH ARTICLE OPEN ACCESS

Effect of Ammonium Polyphosphate/Silicate Content on the Postfire Mechanics of Epoxy Glass-Fiber Composites Using Facile Chocolate Bar-Inspired Structures

Sruthi Sunder[1] | Maria Jauregui Rozo[2] | Sneha Inasu[1] | Dietmar Meinel[2] | Bernhard Schartel[2] | Holger Ruckdäschel[1]

[1]Department of Polymer Engineering, University of Bayreuth, Bayreuth, Germany | [2]Bundesanstalt für Materialforschung Und -prüfung (BAM), Berlin, Germany

Correspondence: Bernhard Schartel (bernhard.schartel@bam.de) | Holger Ruckdäschel (holger.ruckdaeschel@uni-bayreuth.de)

Received: 26 September 2024 | **Revised:** 10 January 2025 | **Accepted:** 12 January 2025

Funding: This work was supported by the Deutsche Forschungsgemeinschaft (AL 474/53-1, SCHA 730/26-1).

Keywords: epoxy | flame retardants | glass fiber composites | postfire mechanics

ABSTRACT

This study investigates the postfire mechanical properties of epoxy glass-fiber reinforced composites (EP GFRCs) using increasing concentrations of ammonium polyphosphate (APP) and inorganic silicate (InSi) to modify the char and fire residue. A facile chocolate bar-inspired structure was introduced for fire exposure and subsequent flexural testing of the GFRCs. The resin matrix used here was a diglycidyl ether of bisphenol-A (DGEBA) resin, cured with dicyandiamide (DICY), and accelerated by Urone. The microstructures of the degraded composites after three-point bending tests, were evaluated using scanning electron microscopy (SEM) and x-ray computed tomography (XCT) imaging. A previous study showed that increasing the APP and InSi content significantly enhanced flame retardancy, via improved char formation under fire conditions. However, flexural properties and fire resistance were adversely affected after fire exposure, highlighting a trade-off effect. Fiber breakage and delamination of the composites increased upon failure with increasing APP + InSi content in the composite due to unconsolidated char. The experimental values for the postfire flexural mechanics were in good agreement with the two-layer model proposed in literature. This paper presents a preliminary basis for postfire mechanical testing of epoxy composites for use in fire-safe structures, using a combination of standardized testing norms.

1 | Introduction

Epoxy (EP) resins and their corresponding glass fiber-reinforced composites (GFRCs) have versatile applications in the construction, transport, medical, and aerospace industries due to their excellent chemical resistance, mechanical strength, and thermal stability [1]. EP GFRCs exhibit excellent flexural properties at room temperature [2, 3] due to the combined contributions of glass fibers (GFs) and the EP matrix. The EP matrix ensures effective stress transfer under bending loads. Flexural modulus and strength are primarily influenced by fiber orientation, volume fraction, and fiber-matrix adhesion, with bidirectional or woven configurations providing balanced properties. Typical flexural moduli range from 20 to 40 GPa, while flexural strength often exceeds 300 MPa, depending on the fiber alignment and matrix stiffness [4]. Failure under flexural loads is governed by mechanisms such as matrix cracking, fiber-matrix debonding, and delamination. Obtaining data on the postfire mechanical properties of these structures is challenging, due to a lack of available standardized testing methods. Postfire mechanical behavior, in

The first two authors contributed equally to this article.

[Correction added on 17 February 2025, after first online publication: The affiliations of all authors have been corrected by switching affiliations 1 and 2.]

conjunction with fire resistance behavior, is essential for applications requiring structural stability after fire exposure, ensuring that residual load-bearing capacity is maintained to allow safer evacuation. While the addition of flame retardants (FRs) is intended to improve the flame-retardant properties of EP resins, GFs [5, 6] can be used to improve the flame retardancy via increasing thermal inertness, and fire resistance simultaneously. Thermal inertness here, refers to the material's resistance to thermal degradation, expansion, or deformation under fire exposure which is an inherent property of the glass reinforcements. Here, the term flame retardancy is specifically used to refer to the ability of a material to resist ignition and to slow down or prevent the spread of a fire. The term fire resistance is used to refer to the ability of a material to maintain its structural integrity while limiting the temperature rise on the side unexposed to a flame [7, 8]. Structural integrity refers to the material's ability to sustain its designed load while minimizing deformations, both during and after fire exposure, ensuring safety and functionality in fire-prone applications. The term "postfire" is used in this study to signify events happening after fire exposure. Various solvent-free FRs acting in the condensed and gas phase exist in the state of the art [9, 10]. Specifically, the combination of ammonium polyphosphate (APP) and inorganic silicate (InSi) can be used to improve barrier and char formation via intumescence of APP, and glassy surface residue formation via melting and reconsolidation of InSi [11–13]. Studies on the transferability and efficacy of FRs in GFRCs versus the resins are challenging [9, 14, 15]. In previous studies [16, 17], we reported on the dramatic decrease of fire residue (char) thickness upon transferring APP and InSi loaded at 10% w/w, 8:2 ratio, in a diglycidyl ether of bisphenol-A (DGEBA) resin to unidirectional (UD) and bidirectional (BD) GFRCs. The fire residue thickness remaining on the composites after cone calorimeter tests was found to be only 10% that of the resins. The challenges in measuring the flexural properties of the structures post-furnace exposure at 400°C due to structural delamination were highlighted. A similar study by Kim and coworkers [15] compared the heat damage on the impact behavior from furnace-exposed DGEBA/flax composites and EP/GFRCs containing melamine coated APP, at 20% w/w, and found increased delamination of the composite structures. Recent studies by Vetter et al. [18] utilized exposure fluxes of 50 and 500 kW/m^2, respectively, over various time intervals, to extensively characterize the decomposition mechanisms in carbon fiber reinforced composites (CFRCs). Bibinger et al. additionally performed tests using heat fluxes ranging from 50 to 1750 kW/m^2 [19]. A three-region model was proposed for the determination of the postfire flexural modulus of the composites based on the area and progression of the damaged regions across the carbon plies. Previously, Mouritz et al. [20] investigated the degradation in the mechanical properties of GFRCs containing various matrices and reinforcements subjected to a heat flux of 50 kW/m^2 using cone calorimeter tests with exposure times from 15 to 240 s. They proposed a two-layer model considering a charred and unburned layer for the theoretical evaluation of the residual postfire modulus which will be evaluated against the experimental data in this investigation. The differences to the three-layer model (see Section 3.5) proposed by Bibinger [19, 21] will additionally be considered. The thickness of the composites studied ranged from ~4.5 to 7.5 mm with fiber volume contents varying from 14% to 34%. Another study conducted by Toubia, Morgan, and Elmushyakhi [22] used cone calorimetry and subsequent flushing of the samples with liquid N_2 to extinguish the flame after cone exposure corresponding to the freeze–thaw cycles in a marine environment. Other studies utilized different types of thermoplastic [23–27] or thermosetting matrices using various types of reinforcements, with FRs [28–31], and without FRs [32] to report on the postradiation or postfire mechanics of composites either via theoretical models [33], or experimentally [22]. The use of a cone calorimeter for fire exposure requires an initial spark time and the composite surface already experiences a heat flux of 30–50 kW/m^2 before ignition. Interrupting or quenching the samples during a measurement is challenging for the operator and might cause thermal damage to the cone heater. Here, we consider a fuel burner in a room atmosphere similar to the method by Mouritz et al. [34]. In this study, a facile chocolate-bar inspired structure is used for fire exposure, focusing on the postfire behavior of EP GFRCs modified with APP and InSi. The APP and InSi in the ratio of 8:2 are thus added in increasing proportions by weight (10%, 30%, and 50%) in a DGEBA resin cured with dicyandiamide (DICY) accelerated by Urone [35, 36]. Composites with a fixed thickness of ~4.3 ± 0.2 mm with a fiber volume fraction of ~55% are studied for correlations with processing parameters [37], flame retardancy, fire resistance, and postfire mechanics. The postfire flexural behavior is evaluated in the context of the morphological properties of the fire residues using scanning electron microscopy (SEM) and x-ray computed tomography (XCT) imaging. Flexural properties were selected as the focus of this study because they represent a combination of tensile, compressive, and shear behaviors, which are critical under bending loads commonly experienced by structural components in real-world applications. Flexural testing provides a measure of fire-induced degradation, capturing effects such as matrix cracking, fiber-matrix debonding, and delamination. This study is thus aimed at developing a potential preliminary basis for the postfire flexural testing of composites, and consequently, testing composites for use in fire-safe structures. This is implemented using facile chocolate bar-inspired structures to study the effect of increasing APP/InSi content on the postfire mechanics of the GFRCs.

2 | Experimental Section

2.1 | Materials and Methods

2.1.1 | Resin and Composite Production

The FR resin system based on DGEBA resin (DER 331-Olin Epoxy) DICY (DYHARD 100S Alzchem) + Urone (DYHARD UR400-Alzchem) in the ratio 100:6.5:1 is prepared using the details explained in previous studies [16, 37]. The same studies provide detailed processing data on the FR processing in the resin and the resulting dynamics upon transfer to the composites. The final fiber volume content in the composites after curing, was maintained at ~57% ± 5%. The APP (FR CROS 484-Budenheim) used in combination with InSi (Flamtard V100-William Blythe) was maintained in the ratio of 8:2 in the resin at loadings of 10%, 30%, and 50% w/w. The BD GFs used (fibers G600BD-1300/Saertex GmbH) had an overall aerial weight of 600 g/m^2, and comparable aerial weights of the fibers in the 0° and 90° directions. For this study, specimens for prefire mechanical testing, post-furnace mechanical testing, fire resistance, and postfire

mechanical testing were sourced from separate batches to ensure independent evaluations. Each batch was prepared under identical processing conditions as reported previously [16, 37] to minimize variability due to manufacturing. The replicate tests within each condition were conducted on specimens cut from a single production batch.

2.1.2 | Sample Preparation Method for Postfire Mechanical Testing of Composites

In this study, we introduce an adapted sample preparation method for composite laminate specimens, inspired by the functional segmental division that allows easy separation from initially joined and packaged structures found in commercial chocolate bars as shown in Figure 1.

The rationale behind this technique is to significantly reduce the influence of edge effects from fire exposure on sample bars required for three-point bending tests. Specifically, this refers to the influence of sample thickness on thermal damage. Such samples experience higher matrix decomposition at the exposed edges [38] making the effect of thickness increasingly significant in fire exposure damage, and thus in lowering mechanical performance. The alternative is to use a flat plate for fire exposure and subsequently separate the burned composite into individual bars for flexural testing. However, this poses two additional challenges. First, the edges of the individual bars which will eventually be separated from the plate would experience lower thermal damage from direct fire exposure, and higher damage due to conduction effects from the front face of the sample. Separating the sample bars from an intact plate after fire exposure subjects the sample to additional sawing stresses which results in further sample damage before mechanical testing that is difficult to quantify. These high sawing stresses result in significant damage to the samples causing additional delamination and fiber breakage making them less viable for flexural testing.

A laminate with a uniform thickness of 4 mm was initially dimensioned into a square shape measuring 100 mm on each side. Prior to mechanical testing, each specimen was subjected to a partial cutting process using a diamond edged saw blade cooled with a water spray. This process was guided by the protocols detailed in Section 2.1.4 for the three-point bending test.

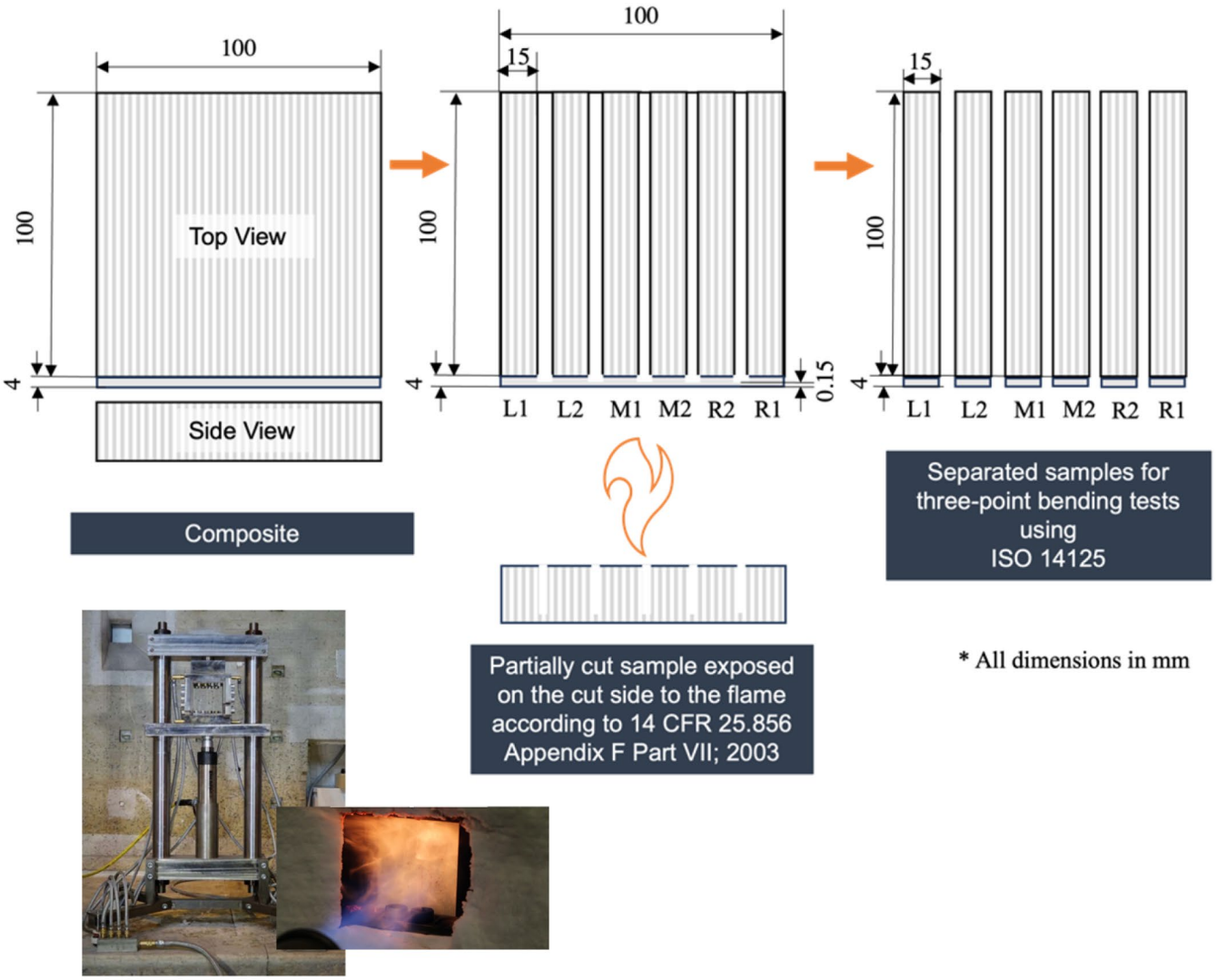

FIGURE 1 | Schematic representation of the segmented composites before fire exposure and separation for flexural tests and the bench-scale setup.

The cutting was executed in such a manner that ~0.15 mm of the laminate remained intact on one face, effectively leaving a thin, uncut layer that connects the sections. After creating the partial cuts, the specimen's partially cut side was exposed to a controlled fire to simulate realistic conditions of flame spread as described in Section 2.1.5. The fire exposure was performed on the cut side rather than the uncut side to ensure partial burning of the edges, while complete delamination due to edge burning is prevented by the ~0.15 mm left uncut. It was observed visually, that the regions left uncut sustained nearly no fire damage. The combined thickness of the grooves make up ~3%–5% of the whole composite length. They are not part of the finally separated structures and are primarily used to introduce edge burning while allowing ease of cutting. However, the potential limitations of the inclusion of these grooves are elaborated in Section 3.7. The fire exposure was conducted in a well-ventilated and controlled environment to prevent excessive smoke inhalation and potential exposure to hazardous combustion products. Additionally, flame spread was observed closely, and safety protocols for handling any unforeseen fire hazards were strictly followed. To further ensure the safety of all personnel involved in the fire exposure and subsequent testing, appropriate safety equipment was used. This included the use of protective glasses, masks, and lab coats to safeguard against potential heat exposure, smoke inhalation, and any other risks associated with the fire testing environment.

After the fire exposures, the specimens were fully separated from the main body of the composite plates by careful sawing. Minimum additional delamination occurred during the sawing process. Each separated specimen was subjected to three-point bending tests with the load applied such that it first encounters the burned surface of the material.

A bench-scale testing apparatus as described in [39–41] was utilized to expose the composites to a controlled flame. The specimens are clamped at the top and the bottom of the apparatus and guided along the side edges. The clamps and guides exposed to fire were equipped with an integrated water-cooling system to prevent unintended thermal expansion. The test samples, as described in Section 2.1.2, were exposed to a heat flux of 30 kW/m^2 for 3 min, and additionally, 50 kW/m^2 for time intervals of 1, 3, and 5 min, respectively. Based on the extent of damage after fire exposure of burned samples (or the spread of the degraded surface), a heat flux of 50 kW/m^2 at 5 min was chosen for the exposure of the samples used for postfire mechanical testing. The samples were burned at 30 kW/m^2 for 3 min were tested postfire to compare the flexural properties at lower fire exposure conditions. The burner was immediately removed after the exposure time was reached, and all samples experienced only a minimal afterglow time of ~5 s. After exposure to these conditions, the sample was extracted for detailed examination using SEM and for mechanical evaluation via three-point bending tests. The bottom of the sample holder covers ~2 mm of the sample length from flame exposure which prevents complete delamination in the event of eventual edge burning effects. The samples were labeled according to their relative positions on the segmented composite from the center. “R” for the segments on the right side; designated as R1 and R2, “L” for the sample segments on the left side; designated as L1 and L2, and finally “M” for the sample segments in the middle; designated as M1 and M2.

2.1.3 | Furnace Exposure of Samples

The samples were prepared according to the details in Section 2.1.2 and placed individually in a muffler furnace oven placed in a fume hood with the uncut sides of the samples in contact with the oven base. The furnace was preheated to a temperature of 400°C at a temperature gradient of 4°C/min before the samples were placed inside. The temperature for the furnace exposure was chosen based on the possibility of exposing the samples for at least 1 min ensuring sufficient damage to the samples without complete delamination or burn-off of the resin. Initial tests were conducted for this purpose beginning at a temperature of 200°C, with steps of 50°C. Lower temperatures (200°C–350°C) were found to confer surface damage without penetrating the bulk of the sample. Higher exposure temperatures (450°C–700°C) presented challenges with obtaining intact samples for testing and greatly increased smoke output which risked damage to the fume hood. The samples were left inside for 1, 2, and 3 min before removal from the furnace. They were allowed to cool down to room temperature before separation of the samples from the overall structure and further testing.

2.1.4 | Three-Point Bending Tests of Resins and Composites

For the analysis of the flexural behavior of the resins, six specimens with dimensions 80 mm × 10 mm × 4 mm were tested using a three-point bending apparatus. The machine was set up according to ISO 178 using a crosshead speed of 2 mm/min on a Zwick Roell Z020 originally from Zwick Roell GmbH & Co. KG (Ulm, Germany). The capacity of the load cell used was 20 kN. The composite samples were similarly analyzed using the DIN EN ISO 14125 standard with dimensions of 100 mm × 15 mm × 4 mm. The load was applied in a transverse direction to the fibers in the 0^o direction of the 0^o/90^o BD composites. The samples subjected to the flame were tested with the exposed (burned) side up.

2.1.5 | Fire Resistance Tests

The fire resistance test was based on procedures from previous studies on carbon-fiber sandwich panels and carbon-reinforced polymer composites [40, 41]. An initial cold test at room temperature determined the ultimate failure load for the composite without FRs E100:GF-BD (78.8 kN), from which 10% (7.8 kN/20 bar) was used for the fire resistance test. The test involved applying a static compression load horizontally at 10% of the cold test failure load. Specimens (120 mm × 120 mm × 4 mm) were exposed to fire vertically with controlled conditions: heat flux of 180 kW/m^2, temperature of 1000°C, propane gas flow of 15 L/min, and a 30.5 cm burner-sample distance. The setup included water-cooled clamps and sides to prevent thermal expansion, with heat flux and temperature calibrated by a Vatell Thermogage TG1000-1. Temperature at the unexposed surface of the specimens was measured using a type K thermocouple. A hydraulic machine applied the compressive load, monitored by the TRACE DAQ software. When compression failure was detected, the load was released, and the burner was reset. All test parameters were kept constant for all trials. Additionally, temperature to failure and time to failure of all the samples were measured.

2.1.6 | Dynamic Mechanical Thermal Analysis (DMTA)

DMTA was conducted on a Gabo Eplexor 500 N in torsional mode. Measurements were performed across a temperature range from 25°C to 180°C (ramp of 3 K/min) on specimens with dimensions of 50 mm × 10 mm × 2 mm. The glass transition temperature (T_g) was identified by determining the peak of the loss factor (tan δ). Each sample type underwent testing with three specimens.

2.1.7 | Postfire Sample Morphology

The burned surfaces of the composite samples containing varying amounts of FRs, exposed at 50 kW/m^2 for various exposure times were analyzed using a Zeiss Gemini 1530 Scanning Electron Microscope from Carl Zeiss AG. The sample surfaces were sputtered using platinum up to a thickness of 5 nm. An acceleration voltage of 3 kV was used. The samples exposed at 30 kW/m^2 for 3 min showed highly inconsistent decomposition across their surfaces, and thus were not analyzed for their microstructure since it was difficult to obtain a representative sample. This is directly linked to the diameter of the flame used for the exposure which is linked to the heat flux applied to the sample. A higher flux implies a higher flame spread onto the sample surface. For the samples exposed at 50 kW/m^2 for 5 min, a representative sample was taken from the center of the exposed structure where the impact of the flame was the strongest.

2.1.8 | XCT

A Diondo d2 MAX Cabrio double-tube CT system from Diondo GmbH, Hattingen, Germany, was used for XCT. The x-ray source was a 240 kV microfocus x-ray tube XWT-240-SE from X-Ray WorX GmbH, Germany. The detector is an amorphous silicon detector panel NDT1717M2/IL with 3000 × 3000 pixels. The CT images were taken in the centre part of the approximately 4-mm-thick sample after exposure to fire and flexural test. The set x-ray energy was 80 kV at a current of 250 μA. The image resolution was 7 μm^3 and the images were analyzed using VG Studio MAX software, version 2023.1 from Volume Graphics GmbH (Heidelberg, Germany). XCT imaging was done using an x-ray source with a 240 kV microfocus x-ray tube XWT-240-SE from X-Ray WorX GmbH, Germany. Approximately 4 mm of the center part of the samples postfire exposure and post-flexural testing were imaged. X-rays were converted into visible light via a scintillation layer using a 3000-pixel × 3000-pixel amorphous silicon detector panel NDT1717M2/IL. The images were evaluated using VG Studio MAX 2023.1 from Volume Graphics GmbH (Heidelberg, Germany). The image resolution was 30 μm^3.

3 | Results and Discussion

3.1 | Determination of Exposure Time at 50 kW/m^2

Although completely homogenous damage to the samples cannot be guaranteed in a fire, the extent to which the sample is damaged can be controlled by adjusting exposure time [42]. The composites in this study could not be exposed for more than 6–7 min without delamination. Figure 2 shows the top surface and microstructures (Figure 3) of the BD GFRCs with 8% APP and 2% InSi content in the DGEBA + DICY + Urone resin after fire exposure at 50 kW/m^2 at three different exposure times. After 1 min of flame exposure the surface exhibits nearly no signs of thermal decomposition apart from discoloration and minor char formation along the edges of the sample sections at the center (Figure 2a). The corresponding SEM image shows signs of initial thermal decomposition with some fiber-matrix debonding visible (Figure 3a). Microcracks and minor voids are visible, indicating the onset of thermal decomposition of the matrix.

After 3 min of exposure, significant surface damage is evident, especially in the top half of the sample uncovered by the clamps, with a noticeable increase in the charred area (Figure 2b). The central region of the composite shows intense blackening compared to the edges, indicating deeper thermal penetration and decomposition of the matrix material. The microstructure in Figure 3b shows increased matrix decomposition, with larger voids and cracks permeating the surface.

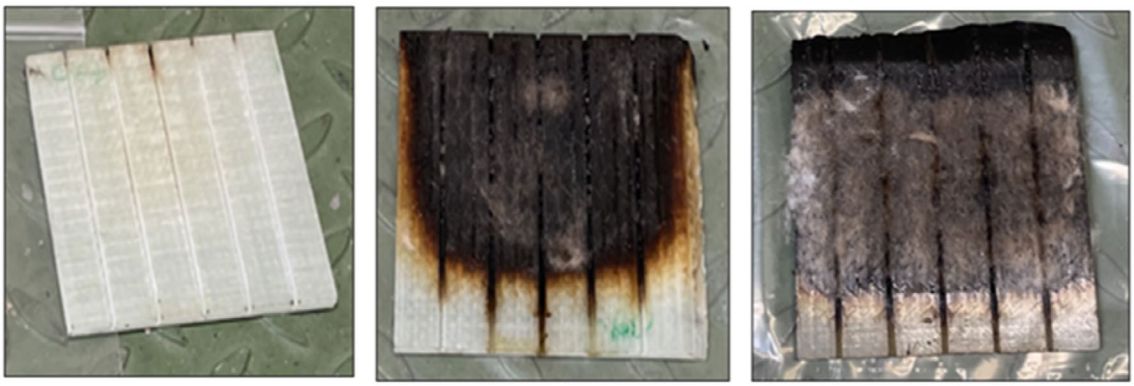

FIGURE 2 | Comparison of the surface structures of the sample surfaces after fire exposure at different times at a fixed heat flux of 50 kW/m^2.

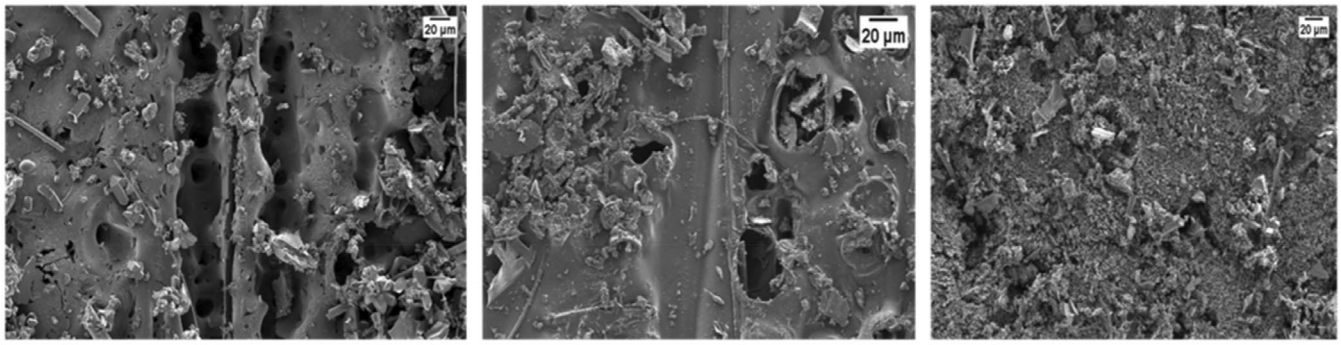

FIGURE 3 | Comparison of the microstructures of the sample surfaces after fire exposure at different times at a fixed heat flux of 50 kW/m^2.

The char residue is more prominent than after 1 min of exposure, indicating an advanced progression of pyrolysis. After 5 min of exposure the composite surface is extensively charred and blackened, which can be attributed to the carbonaceous char of the resin matrix [43] as well as the char formation by the APP [44] (Figure 2c). The integrity of the surface is severely deteriorated, with visible delamination at the top edges, and extensive formation of char residue across the entire surface. The exception to this is a ~2 cm section of the sample at the bottom which is covered by the sample holder during fire exposure. This section of the sample is not in contact with the load during the three-point bending tests and is at the edge of the sample holder during mechanical tests. Thus, the effect of this unburned section is negligible. The SEM image depicts a severely compromised microstructure after prolonged exposure to the flame (Figure 3c) (see Supporting Information for top view images of the samples). The surface is covered with a thick layer of char, and large voids and cracks dominate the microstructure, indicating extensive thermal decomposition and loss of material integrity through a combination of increasing thermal and thermomechanical stresses. The presence of APP in the composite promotes the formation of a protective char layer with increasing exposure times to the flame. Prolonged exposure to 50 kW/m^2 for 5 min allows sufficient decomposition to evaluate the thermal stability and structural integrity of the composite materials. Notably, the use of lower heat fluxes significantly raises the ignition time of GFs, further impacting the start of the thermal decomposition process [42]. This duration enables the assessment of how the material can maintain its mechanical properties postfire without complete delamination. In the absence of FRs in E100:GF-BD, significant thermal decomposition, characterized by fiber-matrix debonding and extensive matrix cracking is visible (Figure 4a). The char layer formation is minimal, and the underlying fibers are exposed, indicating insufficient FR action. E90InSi2APP8:GF-BD shows improved char formation compared to E100:GF-BD (Figure 4b). The matrix retains better integrity, and fewer fibers are exposed. The increased char layer acts as a thermal barrier, improving the flame retardancy of the composite. At 30% FRs, E70InSi6APP24:GF-BD shows a substantial loose char layer that covers the fibers, significantly reducing the exposure of the underlying material (Figure 4c). Fewer samples show signs of matrix cracking and debonding, with an increase in porous char.

Further increasing the FR content to 50% in E50InSi10APP40:GF-BD shows that extensive char formation is evident, which completely covers the fibers (Figure 4d). The thick, cohesive char layer indicates the effectiveness of high APP + InSi content in enhancing FR action. These observations are in-line with the quantified modes of action of the FRs from cone calorimeter studies in the composite structures previously reported by the authors [36]. The progressive damage represented in these images, correspond with observations in the state of the art describing matrix decomposition, and char formation due to the APP, in addition to fiber-matrix interface, leading to matrix softening, cracking, debonding, void formation, and eventual structural failure [44, 45].

3.2 | Prefire Mechanics of the Resins Versus Composites and Postfire Mechanics of Composites

Figure 5 displays the flexural modulus of the composites are expectedly eight times higher than that of the resins due to the high fiber volume content at ~55% (or ~75% by weight) which is in agreement with data reported in literature [45]. As shown in, the flexural modulus and flexural strength of the composites are strongly negatively correlated with increasing combined APP + InSi content with r values of −0.96 and −1, respectively. The flexural strength of the resins is strongly negatively correlated with increasing FR content with an r value of −0.88, however, the flexural modulus is strongly positively correlated with an r value of +0.94. This can be explained by the decreasing flexural strain with increasing FR content with an r value of −0.974. In the resins, the addition of the APP and InSi as solvent-free fillers, introduces points of stress concentration and potential defects, which weaken the material and reduce its ability to withstand flexural loads (Table 1).

The high cross-linking density of pure EP materials compromises their toughness and impact resistance, leading to an inherent brittle structure, susceptible to crack initiation and propagation [46]. The FR additives disrupt the resin matrix continuity and reduce the effective load bearing area. Despite the decrease in strength, the decrease in flexural modulus of neat resins can be attributed to the fillers making the resin matrix

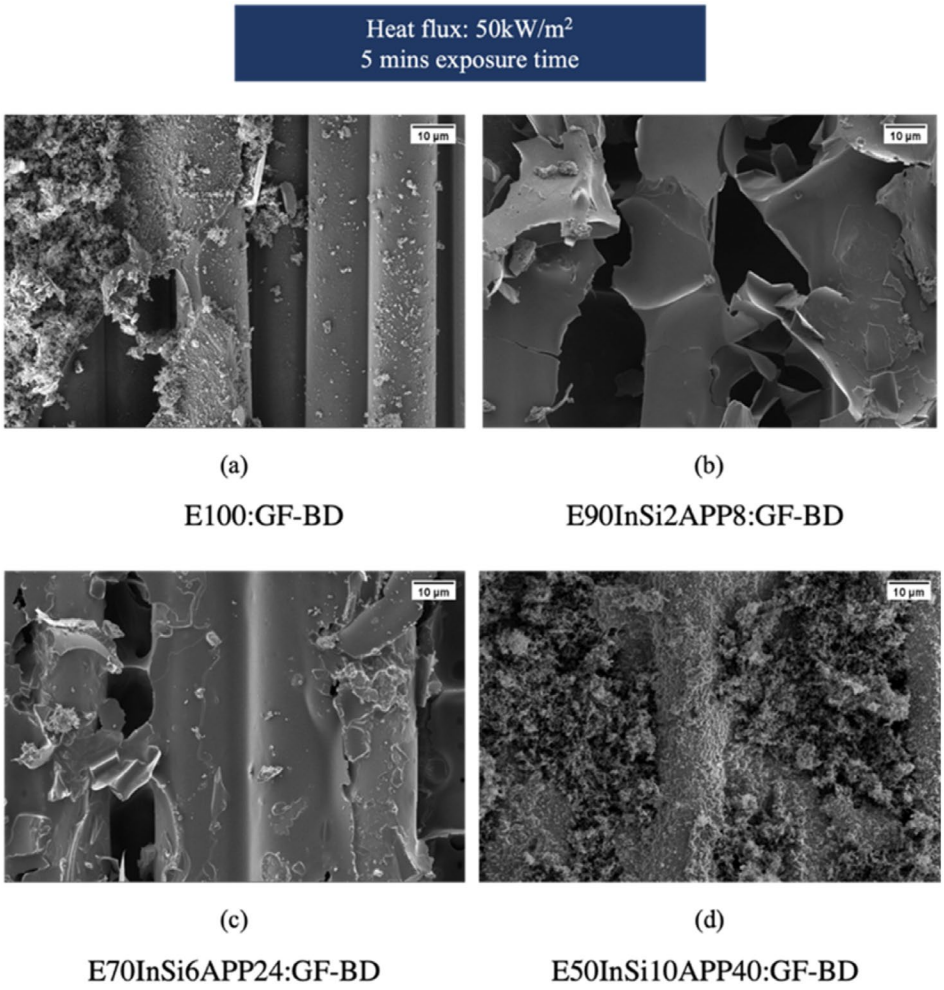

FIGURE 4 | Comparison of the microstructures of the composites containing varying amounts of APP + InSi at a fixed heat flux of 50 kW/m^2 for 5 min.

more rigid. The rigid particles restrict the deformation of the matrix, leading to a higher modulus [47, 48].

In contrast, the flexural modulus of composites decreases with increasing FR content since the presence of fillers can lead to detrimental effects in the composites. These effects include interference with fiber-matrix bonding reducing the efficiency of load transfer, as well as agglomeration and voids within the inter and intratow regions of the composite with increasing FR additive content. This is supported by the SEM data previously reported by the authors and in findings in literature [46, 48–54]. Notably, Rajaei, Wang, and Bhattacharyya [55] and Riahipour et al. [49] reported a similar decline in the mechanical strength of the resins and composites due to APP which was improved using additional fillers such as talc and silica.

3.3 | Post-Furnace Mechanics of the Composites

Figure 6 shows the changes in flexural strength, strain at failure, and flexural modulus of GFRCs with increasing (APP + InSi) content after furnace exposure. The flexural strength of the BD composites decreases significantly after exposure to furnace conditions for 1 and 2 min, across all the composites tested. For the sample E100, a significant reduction in flexural strength is observed, dropping from approximately 800 MPa pre-furnace to below ~600 and ~ 500 MPa after 1 and 2 min of furnace exposure, respectively. Similar trends are seen in E90InSi2APP8:GF-BD and E70InSi6APP2:GF-BD, though the rate of decrease is less severe compared to E50InSi10APP40:GF-BD. E100:GF-BD exhibits a marked decrease in strain, highlighting the embrittlement of the composite after thermal exposure. All the composite samples exhibit similar reductions in strain. This suggests that the higher InSi content contributes to significant embrittlement making it more prone to failure under stress. For all samples, flexural failure occurred in conjunction with matrix cracking, with fine cracks visible on the underside of the samples where the applied load was the highest. Localized buckling of the fibers due to compression was observed. Complete breakage of the samples was not observed, despite significant deformation. The flexural modulus of the composites displays a varied response to furnace exposure.

For E100:GF-BD, the flexural modulus decreases significantly, indicating a reduction in stiffness due to thermal effects. E90InSi2APP8:GF-BD follows a similar trend, though with a noticeable reduction after 2 min compared to initial exposure. In contrast, E70InSi6APP24:GF-BD shows a less noticeable reduction in the flexural modulus post-furnace exposure compared to the other BD composites, suggesting some degree of thermal

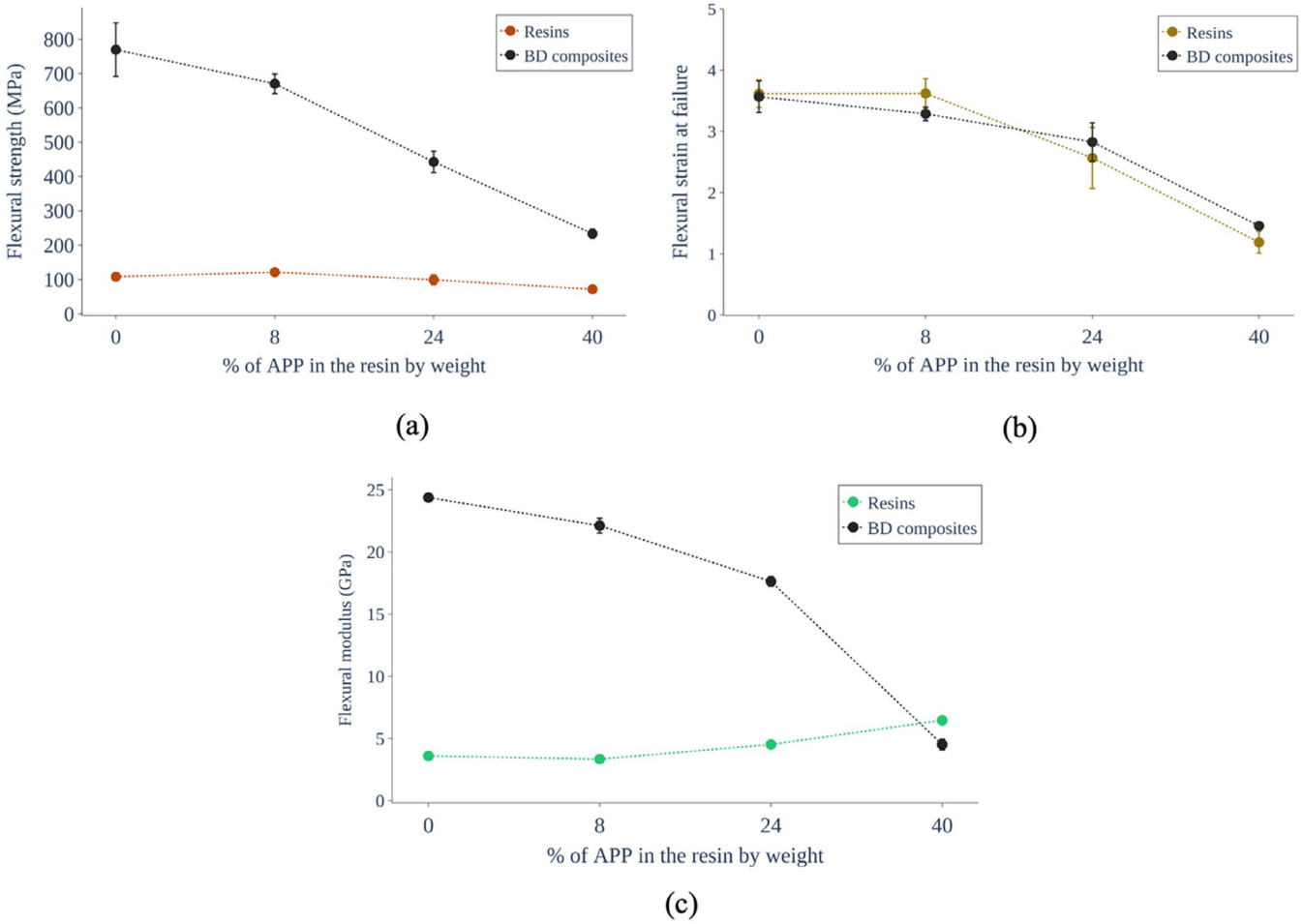

FIGURE 5 | Comparison of the impact of increasing FR content on the flexural properties of the resins and composites.

TABLE 1 | Flexural properties of the resins and composites at room temperature.

Resin formulation	% w/w APP in resin	E_F^{resin} (GPa)	E_F^{RT} (GPa)	σ_F^{resin} (MPa)	σ_F^{RT} (MPa)	ε_F^{resin}	ε_F^{RT}
E100	0	3.6 ± 0.2	24.4 ± 0.3	108.1 ± 8	769.5 ± 78	3.6 ± 0.2	3.6 ± 0.3
E90InSi2APP8	8	3.3 ± 0.2	22.1 ± 0.6	121.3 ± 9	670.2 ± 28	3.6 ± 0.2	3.3 ± 0.1
E70InSi6APP24	24	4.5 ± 0.1	17.6 ± 0.4	99.1 ± 15	442.5 ± 31	2.6 ± 0.5	2.8 ± 0.3
E50InSi10APP40	40	6.5 ± 0.1	4.5 ± 0.4	71.4 ± 10	233.2 ± 13	1.2 ± 0.2	1.5 ± 0.03

stability imparted by the FR content. In E50InSi10APP40:GF-BD, the modulus shows a marked increase, indicating that while flexural strength and strain suffer, the stiffness is less affected by the thermal exposure. This increase in modulus is attributed to the FRs that are distributed extensively across the composite structure [37], which balance out some of the thermal decomposition effects. The observed reduction in flexural strength and strain at failure across all composites post-furnace exposure can be attributed to the decomposition of the EP matrix. Exposure to high temperatures as expected, would lead to the pyrolysis of the EP chains, resulting in a loss of mechanical integrity [56]. The introduction of APP as an FR and InSi as an additive, while beneficial for flame retardancy, worsens the degradation of the mechanical properties due to loose char formation, leading to significant reductions in mechanical performance. The higher FR content in E50InSi10APP40:GF-BD corresponds with a substantial decrease in both flexural strength and strain at failure, indicating significant embrittlement [57]. This suggests that while the FRs may contribute to thermal stability and increase rigidity, they cause embrittlement due to the higher InSi (glass) content in this composite. A proposed schematic of this concept is given in the Supporting Information. The FR content negatively impacts the composite's ability to withstand mechanical stress and causes faster failure. A crucial factor to consider here is the matrix–fiber interaction which degrades due to the high thermal stress, compromising load transfer [20]. At 3 min of furnace exposure, the samples were already breakable by hand and could not withstand the sawing stresses required for sample preparation. The use of direct flame contact described in Section 3.4 compared to the furnace exposures, represents a more intense condition with

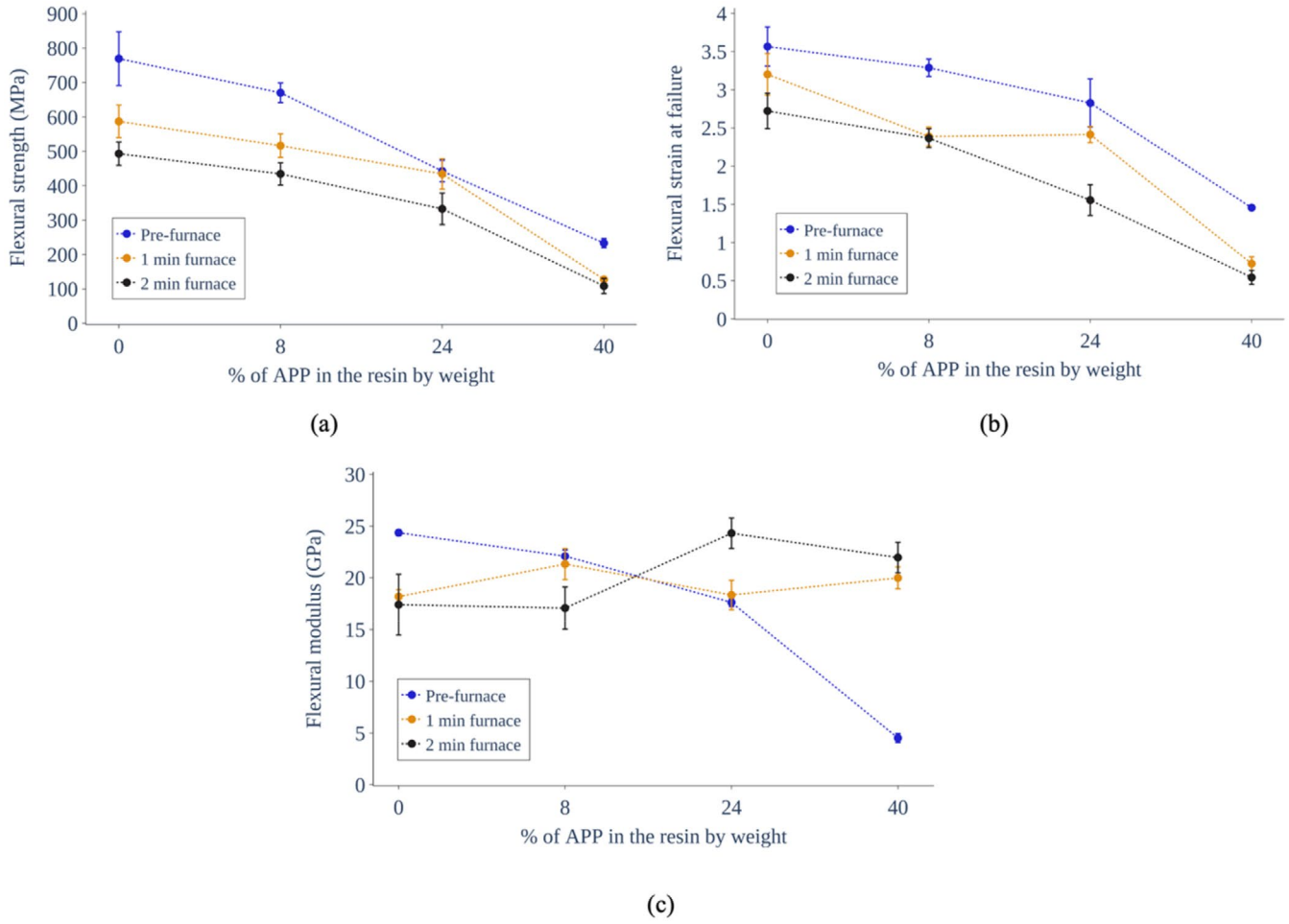

FIGURE 6 | Post-furnace flexural modulus (a) strength (b), and strain (c) after varying furnace exposure times at 400°C and APP + InSi content.

combined convective and radiative heating. However, composite materials may experience radiant heating from nearby burning objects (in the presence of oxygen), which produces a more moderate and sustained thermal load. This produces differing residues with oxidising char as evidenced by the differences in the reported post-furnace and postfire flexural behaviors.

3.4 | Postfire Mechanics of the Composites

Figure 7 and Tables 2–4 show the changes in flexural strength, strain at failure, and flexural modulus of GFRCs with increasing (APP + InSi) content after fire exposure at 30 kW/m^2 for 3 min and 50 kW/m^2 for 5 min.

The flexural modulus of the composites shows a distinct response to fire exposure, as compared to furnace exposure ($r = -0.90$). For E100:GF-BD, the modulus decreases significantly with increasing heat flux and exposure time, highlighting the thermal decomposition of the composite structure under fire conditions. This trend is consistent with E90InSi2APP8:GF-BD and E70InSi6APP24:GF-BD, where higher heat fluxes and longer exposure times lead to significantly lower flexural moduli. E50InSi10APP40:GF-BD exhibits a relatively stable modulus at lower heat fluxes, but a sharp decline is observed at 50 kW/m^2 after 5 min, indicating the onset of significant fire damage. This behavior contrasts with the furnace exposure, where the modulus of E50InSi10APP40:GF-BD increased, suggesting that the fire exposure impacts the composite more severely as shown in Figure 4. The flexural strength similarly declines with increasing heat flux and exposure time across all samples.

The flexural strain at failure shows varied responses among the samples. E100:GF-BD and E90InSi2APP8:GF-BD display a substantial reduction in strain with increased heat flux and time, indicating increasing brittleness under fire conditions. For E50InSi10APP40:GF-BD and E70InSi6APP24:GF-BD, the flexural strain remains relatively stable at lower heat fluxes but rises sharply at the highest flux, pointing toward sudden flexible behavior. This differs from furnace exposure, where strain decreased more consistently across all samples, reflecting the more controlled environment of furnace testing and the difference in residue. The trends observed reflect those observed in other studies in literature. However, here the heat flux and time of exposure used are slightly higher than the limits tested in the state of the art (see Supporting Information). Despite the significant degradation in flexural properties, the high fiber volume content present in the composites results in the measured residual flexural modulus postfire exposure at 50 kW/m^2 for 5 min ranging from 0.2 to 3.13 GPa. This is ~2%–5% higher than that of the EP/GF composites reported in literature

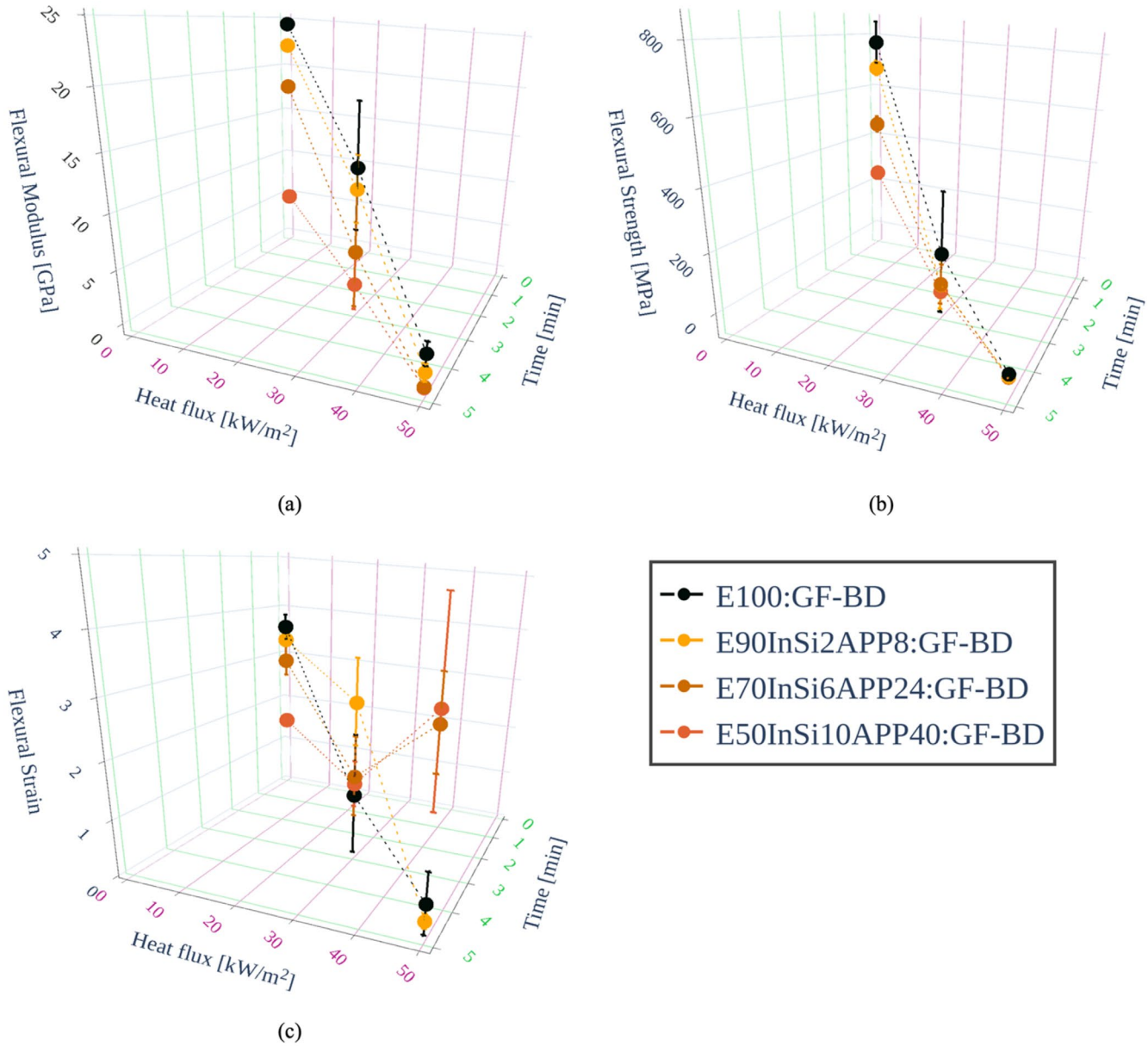

FIGURE 7 | Postfire flexural modulus (a) strength (b), and strain (c) after varying fire exposure parameters and APP + InSi content.

TABLE 2 | Prefire flexural properties of the composites.

Composite	% w/w APP in resin	E_F^{RT} (GPa)	σ_F^{RT} (MPa)	ϵ_F^{RT}
E100:GF-BD	0	24.3 ± 0.3	769.5 ± 78	3.6 ± 0.3
E90InSi2APP8:GF-BD	8	22.1 ± 0.6	670.2 ± 28.5	3.3 ± 0.1
E70InSi6APP24:GF-BD	24	17.6 ± 0.4	442.5 ± 31.3	2.8 ± 0.3
E50InSi10APP40:GF-BD	40	4.5 ± 0.4	233.2 ± 0.43	1.5 ± 0.3

despite the increased heat flux used for the fire exposure [28, 58]. The normalised values of the flexural properties are reported in. $E_F^{30,3}$ decreases the most for E70InSi6APP24:GF-BD although the absolute value is higher than that of E50InSi10APP40:GF-BD. However, $\sigma_F^{30,3}$ decreases similarly for all the samples containing FRs. The trend in the normalized values of $E_F^{50,5}$ and $\epsilon_F^{50,5}$ matches that of the absolute values. However, for $\sigma_F^{50,5}$ the normalized values are similar for all the composites reflecting a correlation between prefire and postfire strength.

Considering the SEM images in Figure 4, it is evident that the looseness of the char further degrades the resin-matrix interface leading to a decrease in the postfire flexural properties. The degradation in the postfire flexural properties overpower the action

TABLE 3 | Postfire flexural properties of the composites at two different exposure parameters. Variability in the sample properties based on relative distances from the center of the flame are reported in the Supporting Information (G).

Fire exposure heat flux/time		30 kW/m², 3 min			50 kW/m², 5 min		
Composite	**% w/w APP in resin**	$E_F^{30,3}$ (GPa)	$\sigma_F^{30,3}$ (MPa)	$\epsilon_F^{30,3}$	$E_F^{50,5}$ (GPa)	$\sigma_F^{50,5}$ (MPa)	$\epsilon_F^{50,5}$
E100:GF-BD	0	13.6 ± 5.8	159.3 ± 215	1.2 ± 1.1	3.1 ± 1.1	13.6 ± 4.4	0.7 ± 0.5
E90InSi2APP8:GF-BD	8	11.6 ± 3.1	47.7 ± 91	2.9 ± 0.7	1.5 ± 0.8	5.6 ± 1	0.4 ± 0.1
E70InSi6APP24:GF-BD	24	5.6 ± 5.6	49.4 ± 73	1.6 ± 0.7	0.2 ± 0.1	4.8 ± 0.5	3.3 ± 0.7
E50InSi10APP40:GF-BD	40	2.3 ± 2.6	21.4 ± 10.6	1.4 ± 0.4	0.1 ± 0.2	3.5 ± 1.4	3.6 ± 1.1

TABLE 4 | Normalized postfire flexural properties of the composites at different exposure parameters.

Composite		30 kW/m², 3 min			50 kW/m², 5 min		
Normalized value (%)	**% w/w APP in resin**	$E_F^{30,3}$	$\sigma_F^{30,3}$	$\epsilon_F^{30,3}$	$E_F^{50,5}$	$\sigma_F^{50,5}$	$\epsilon_F^{50,5}$
E100:GF-BD	0	56	21	33	13	2	19
E90InSi2APP8:GF-BD	8	52	7	88	7	1	12
E70InSi6APP24:GF-BD	24	32	11	57	1	1	118
E50InSi10APP40:GF-BD	40	51	9	93	2	2	240

of the FRs, despite higher loadings of APP + InSi resulting in higher char and protective layer mechanisms on the surface of the composites during cone calorimeter tests [37]. This highlights a parallel in the behavior of EP GFRCs by Bibinger, Eibl, and Gudladt, where the carbon fibers undergo a loss in mechanical performance caused by thermal degradation [21]. Very high standard deviations are observed in the data for moderate flux/time of exposure (30 kW/m² for 3 min; Table 3). Thus, within the scope of this study, it was only possible to obtain a range of values for the postfire mechanics since the composites are extensively degraded. This variability aligns with Bibinger, Eibl, and Gudladt's [19] observations that, as the degree of degradation varies across different layers of the composite, particularly, in regions exposed to nonuniform heat flux, the mechanical response can differ significantly within the same sample. Higher localized temperatures lead to rapid degradation, which disproportionately affects the structural integrity of both CFRPs and GFRPs. Fire exposure combines convection, radiation, and potentially direct flame contact with pressure from the gas flow causing higher localized temperatures and rapid decomposition. This contrasts with the primarily convective heat transfer in a controlled environment in furnace exposure with higher oxidative decomposition. Furnace exposure is thus more uniform, though less intense compared to the fluctuating and often highly localized temperatures in a fire (for a comparison of the sample surfaces see Supporting Information). Hence, although furnace exposure yields more homogenously degraded samples with low standard deviation in the post-furnace mechanical data, fire exposed samples yield more severely, yet less homogenously degraded samples for the evaluation of extreme fire conditions. It is vital to consider that, unlike a controlled setup such as the cone calorimeter, fire may not result in homogenous sample burning which can cause a varied postfire mechanical response depending on the initial proximity to the flame. Consequently, within the scope of this study, the postfire mechanical behaviors of the composites are better represented as a range of values. The stress–strain curves for the samples exposed at 50 kW/m² for 5 min were additionally evaluated for flexural modulus using a linear fit in the strain region of 0.1%–0.3% followed by evaluating the tangent (see Supporting Information).

3.5 | Comparison With the Two-Layer and Three-Layer Model

The experimental values of the postfire mechanics obtained from fire exposure of the samples at 50 kW/m² for 5 min were compared against calculated values of the postfire flexural modulus based on the two-layer model proposed by Mouritz [20]. The values of the postfire flexural modulus are reported directly from the software ($E_F^{50,5}$) and analyzed via the secant method ($\left(E_F^{\text{post\_secant}}\right)$—see Supporting Information D(a)). Additionally, the flexural stiffness $\left(E_{\text{post}}^{\max}\right)$ is reported calculated according to the tangent method (see Supporting Information D(b)). According to the model, the postfire flexural modulus E_F^{post} is calculated using the following equation:

$$E_F^{\text{post}} = \left(\frac{4\left(d-d_n\right)^3 + 4\left(d_n-d_c\right)^3}{d^3}\right).E_F^{RT} \quad (1)$$

where E_F^{RT} is the flexural modulus at room temperature, d is the thickness of the sample in mm, d_c is the thickness of the char layer in mm, d_n is the neutral axis of the beam that is calculated by the equation:

$$d_n = \frac{E_F^{RT}d^2 - d_c^2\left(E_F^{RT} - E_c\right)}{2E_F^{RT}d + 2E_cd_c - 2E_F^{RT}d_c} \quad (2)$$

where E_c is the flexural modulus of the char layer, which according to the model is 0. The model assumes that the thickness of the burned and unburned regions are distinct, that there is no interfacial region where partial decomposition occurs, and that the char layer makes no contribution to the final flexural modulus of the composite. The char layer thickness d_c is difficult to determine visually in the case of the composites used in this study. Hence, the expansion of the composites fire exposure was assumed to be attributed primarily to char/protective residue formation. Thus, the estimated char thickness d_c' was determined as the difference in the thickness of the samples before and after fire exposure as:

$$d_c^{'} = d_{\text{posrt}} - d_0 \tag{3}$$

where d_0 is the average thickness of the composite before fire exposure and d_{post} is the postfire thickness of the composite in mm. The calculated values $E_F^{\text{post\_1}}$ are significantly higher than the expected experimental results (Figure 8).

Based on measurements made of the sample char thickness on the surface, the char layer penetrates beyond the surface into ~1 mm of the composite. Hence, this was modified in Equation (3) and represented as d_c'' . These values are summarized in Table 5. The two-layer model does not consider the contribution of the flexural modulus of the interface between the burned and unburned layers which become increasingly significant with decreasing thicknesses of the samples (see microscopic view of sample edges in Supporting Information). However, it appears that the current approach used to estimate $E_F^{\text{post\_2}}$ based on d_c'' is successful in estimating the postfire flexural behavior of the composites in the expected range reported previously in the literature.

Figure 9 depicts a side view of XCT scans, highlighting the morphological changes induced by fire exposure on the GFRCs using a heat flux of 50 kW/m^2 for 5 min. The imaging was performed on samples after the three point bending tests. Notably, the samples exposed at 50 kW/m^2 for 5 min were already partially delaminated at the top half due to higher intensity of the fire exposure (Figure 9 and Table 5).

Similar to the flexural tests at room temperature, complete breakage upon failure was not observed for any of the samples despite significant deformation and cracking. However, all samples showed fiber breakage, interfacial debonding as well as compression buckling on the sample sections closes to the applied load with the extent of fiber debonding increasing with increased APP + InSi content (Figure 9). The image of E100:GF-BD shows considerable voids and areas of delamination, indicating significant decomposition due to fire exposure. The EP cured with DICY + UR400 as a matrix fails to effectively protect the GFs under the applied heat flux. In the sample E90APP8InSi2:GF-BD, the structure appears more compact with fewer voids. The GFs remain distinct, though there is evidence of reduced resin volume, suggesting that the inclusion of additives improves the thermal stability of the resin matrix to some extent, conferring protective effects. In the sample E70APP24InSi6:GF-BD, the structure shows even fewer pores with better adhesion between the remaining matrix and the fibers. The formed char layer covers significant parts of the resin–fiber interface. This moderate inclusion of APP + InSi significantly improves the fire retardant properties of the composite, maintaining better cohesion between the fibers and the resin despite introducing flexibility from the loose char thus reducing the overall stiffness. This is indicated in the increased strain at failure for this composite, as well as for E50APP40InSi10:GF-BD. To estimate the residual flexural modulus using the three-layer model proposed by Bibinger et al., the following equation is used:

$$\frac{E_{\text{Fres}}^{\text{post\_3}}}{E_F^{\text{RT}}} \approx \frac{\sigma_{\text{res}}}{\sigma_F^{\text{RT}}} = \left(\frac{p_{\text{rIII}}}{p_t}.\alpha_{\text{rIII}}\right) + \left(\frac{p_{\text{rII}}}{p_t}.\alpha_{\text{rII}}\right) + \left(\frac{p_{rI}}{p_t}.\alpha_{rI}\right) \tag{4}$$

where $\frac{\sigma_{\text{res}}}{\sigma_F^{\text{RT}}}$ is the normalized residual strength, p_{rIII}, p_{rII}, and p_{rI} are the percentages of regions rIII, rII, and rI, respectively. p_t is the total area, which is 100% in this case. α_{rIII} represents

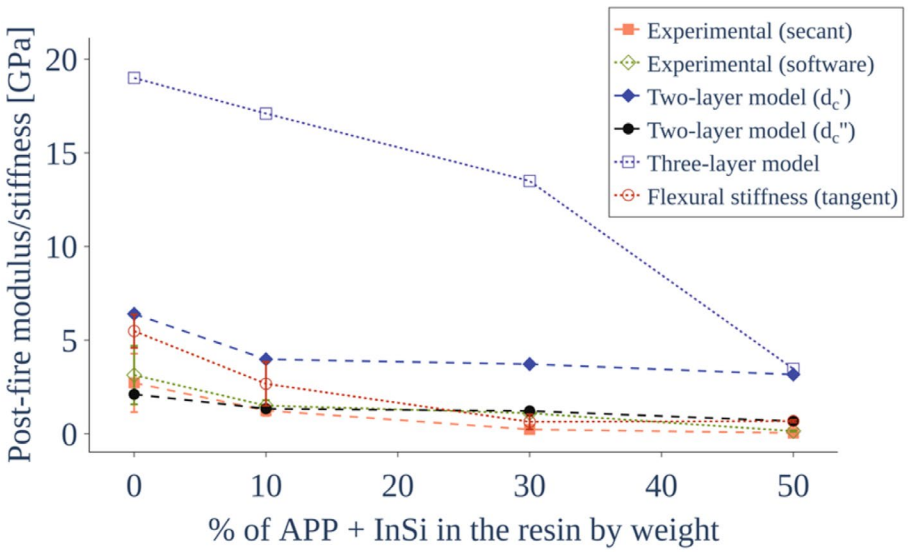

FIGURE 8 | Comparison of measured (fire exposure of 50 kW/m^2 for 5 min) reported experimentally from the data in the Zwick software and by the secant method, flexural stiffness by the tangent method, and calculated postfire flexural modulus from the two-layer model and three-layer model.

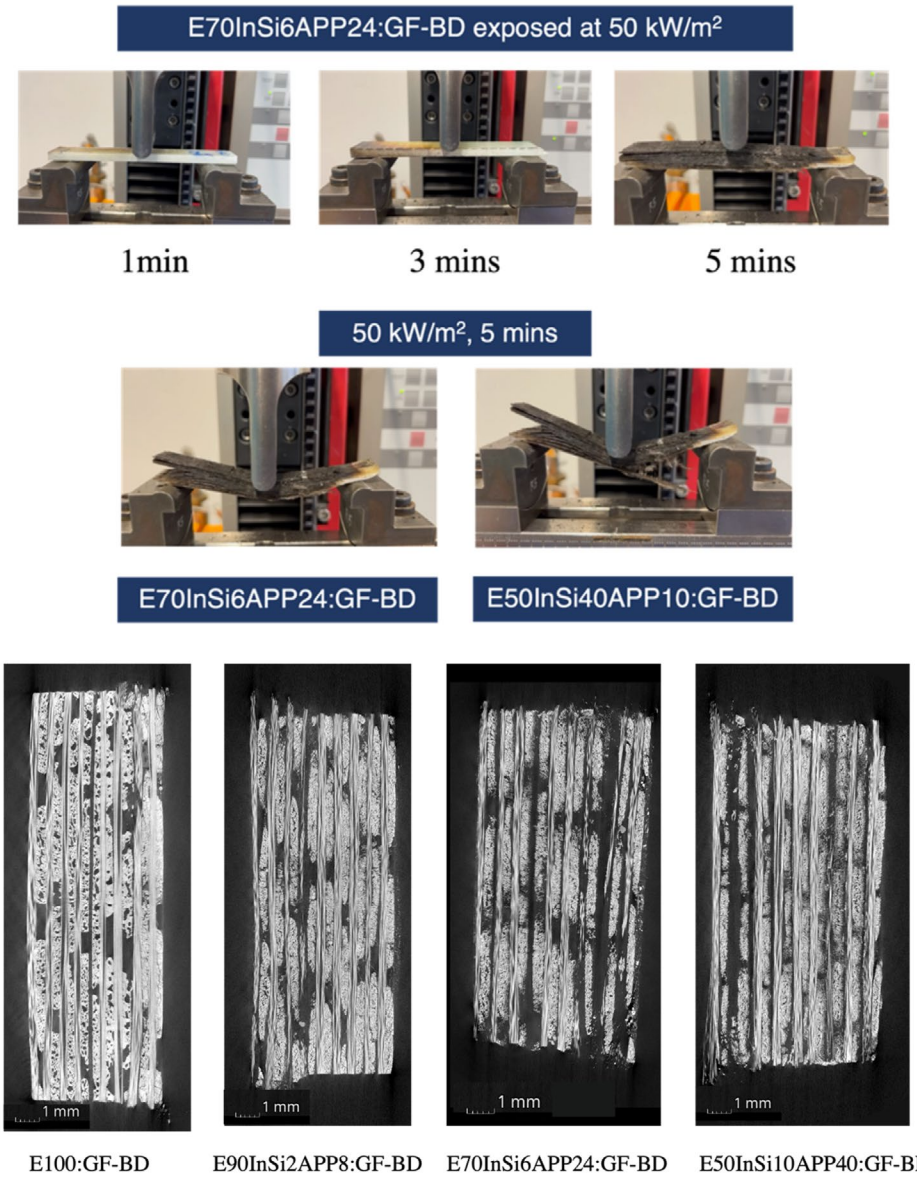

FIGURE 9 | Three point bending testing of burned samples at various exposure times (top) and cross-section of composite specimens after fire exposure and flexural testing with 30% and 50% APP + InSi FR content measured via XCT (bottom) (see Supporting Information for further surface and edge images).

TABLE 5 | Calculated char thicknesses and corresponding theoretical postfire flexural moduli.

Composite	% w/w APP in resin	d_c' (mm)	$E_F^{post\_1}$ (GPa)	d_c'' (mm)	$E_F^{post\_2}$ (GPa)	E_{post}^{max} (GPa)	$E_F^{post\_secant}$ (GPa)
E100:GF-BD	0	1.80	6.4	2.80	2.11	5.5 ± 0.9	1.6 ± 1
E90InSi2APP8:GF-BD	8	2.07	4.0	3.07	1.34	2.7 ± 1.1	0.3 ± 0.8
E70InSi6APP24:GF-BD	24	2.19	3.7	3.19	1.22	0.6 ± 0.4	0.1 ± 0.1
E50InSi10APP40:GF-BD	40	2.39	3.1	3.69	0.67	0.7 ± 0.1	0.03 ± 0.2

undamaged material that contributes fully to the strength. α_{rII} is between 0 and 1 and represents partially damaged material which contributes partially to the strength. α_{rI} is set to 0 and represents severely degraded material which does not contribute to the strength. The various regions are estimated using area analysis in the ImageJ analysis software (see Supporting Information). The comparison between the three-region model and the two-layer model reveals both strengths and limitations in each approach. The three-region model is particularly valuable when analysing composites with distinct damage gradients.

TABLE 6 | Correlation matrix for various parameters obtained in this investigation [37].

	FR content in resin (% w/w/)	E_F^{resin} (GPa)	σ_F^{resin} (MPa)	ϵ_F^{resin}	E_F^{RT} (GPa)	σ_F^{RT} (MPa)	ϵ_F^{RT}	T_g (°C)	T at failure (°C)	$E_F^{50,5}$ (GPa)	pHRR (kW/m²)	$E_F^{post\_2}$ (GPa)
FR content in resin (% w/w/)	1.00											
E_F^{resin}	0.94	1.00										
σ_F^{resin} (MPa)	−0.88	−0.98	1.00									
ϵ_F^{resin}	−0.97	−0.99	0.97	1.00								
E_F^{RT} (GPa)	−0.96	−0.98	0.93	0.99	1.00							
σ_F^{RT} (MPa)	−1.00	−0.95	0.89	0.97	0.96	1.00						
ϵ_F^{RT}	−0.97	−0.98	0.92	0.99	1.00	0.97	1.00					
T_g (°C)	0.65	0.81	−0.79	−0.77	−0.83	−0.64	−0.81	1.00				
T at failure (°C)	−0.95	−0.89	0.87	0.93	0.87	0.96	0.88	−0.47	1.00			
$E_F^{50,5}$ (GPa)	−0.90	−0.71	0.61	0.78	0.77	0.90	0.79	−0.30	0.88	1.00		
pHRR (kW/m²)	−0.99	−0.90	0.84	0.94	0.91	0.99	0.92	−0.52	0.98	0.94	1.00	
$E_F^{post\_2}$ (GPa)	−0.85	−0.65	0.51	0.72	0.75	0.84	0.77	−0.36	0.75	0.96	0.86	1.00

This is seen in the case of carbon fiber composites, where the matrix and fiber interactions are more varied across the damage spectrum at lower exposure times. The difficulty in differentiating the *r*II (partially damaged) region, suggests that the three-region model evaluated by greyscale analysis is challenging. Moreover, the high contrast between the damaged regions and the GFs in the XCT images makes RGB mapping difficult. GFs, unlike carbon fibers, do not form a protective carbonaceous char that can shield the underlying material from further decomposition. Instead, they maintain their structure but fail to provide significant postfire mechanical support once the surrounding matrix has degraded [59]. This difference is crucial as it suggests that the protective effects seen in CFRPs may not fully translate to GFRCs, leading to different postfire performance outcomes. Thus, the three-layer model seems to be reduced to a two-layer model in the current scenario, where the damage distribution is more binary due to the nature of the fibers and matrix. However, the two-layer model more closely matches the experimental data when an interface thickness of ~1 mm is considered, indicating that a three-region model with a different approach to estimating the partially damaged regions may be appropriate here. Machine learning approaches or statistical analysis can more accurately determine the contribution of various components within the GFRCs to the overall residual modulus.

3.6 | Correlations Between FR Content and Material Properties

Table 6 shows a correlation matrix for various critical parameters including FR content, pHRR, T_g , and temperature at failure. The increasing APP + InSi content is strongly positively correlated with an improvement in flame retardancy of the composite via a decrease in the pHRR values ($r = -0.96$). Simultaneously, the postfire flexural modulus starkly decreases with FR content ($r = -0.90$). This trade-off in the influence of the APP + InSi on improving flame retardancy, while degrading the mechanical properties of the composites is important to consider when using char-promoters to improve FR behavior. The capability of increasing gas-phase action over condensed phase action via flame inhibitors, synergists, and the effect of the same on the postfire mechanics of the composites will be evaluated in a future study. Since APP + InSi is additively incorporated into the resin matrix before transfer to the composites which are dominated by the presence of the GFs, the T_g is moderately correlated with FR content, with a value of 0.65. This is reflected similarly with almost no correlation between T_g and the postfire flexural modulus of the composites with $r = -0.30$. The temperatures at failure during the fire resistance test (Table 7) which is indicative of the fire resistance property of the composites, are strongly correlated with their postfire flexural moduli showing that flame retardancy and fire resistance are separate material properties.

3.7 | Future Investigations to Improve Postfire Testing and Analysis

Although the segmented samples are cut with the highest precision possible, certain improvements to the current method are possible. For weaker or thinner composite structures than those presented in the study, the grooves could lead to premature delamination or breakage during or after fire exposure, complicating postfire mechanical testing. Since the groove depth is ~3.8 mm on average, ensuring that segments remain intact for meaningful postfire testing can be challenging at higher fire intensities. Pyrolysis gases may escape laterally through the grooves, altering the char formation mechanism compared to a continuous sample. This can affect the thermal and mechanical behavior of the char layer. However, since the char layer has no contribution to the overall flexural properties, these gases are unlikely to affect the final properties. Nevertheless, the quantification of the release of these gases will be considered in the future. Due to the impact of sawing stresses resulting in damage after fire exposure, a comparison of the proposed method with flat-plate samples was not possible within the scope of this investigation. The transferability of the lab-scale exposure method to larger structures has not been addressed here. Both aspects can be considered for future investigations. Other exposure methods such as cone calorimetry can be considered, keeping in mind the impact to the test apparatus and the safety of the operator from smoke exposure. Batch-to-batch variability resulting from specimens derived from different production batches has not been reported here. Although consistent processing conditions suggest that batch-to-batch effects could be minimal, this will be addressed in future studies. Despite nonlinearities in the flexural behavior of the composites postfire (see Supporting Information), the neutral axes of the bars have been calculated here neglecting these nonlinearities. Although the experimental values and calculated values are in close agreement, in future work, we propose incorporating nonlinear modeling techniques, such as finite element analysis or multilayer approaches, to account for progressive material degradation. Additionally, experimental methods like digital image correlation could be employed to track the neutral axis position dynamically during loading. Finally, deformation-controlled testing was not employed here due to the high variability in degraded composites after fire exposure. However, this could enhance the understanding of postfire behavior and can be considered in future investigations. Within this study, compliance with ISO 14125 norms was maintained to build a foundation for future postfire investigations. However,

TABLE 7 | Temperature at failure measured via fire resistance tests and T_g of the composites via DMA.

Composite	% w/w APP in resin	Temperature at failure (°C)	T_g (°C)
E100:GF-BD	0	75 ± 17	156 ± 6
E90InSi2APP8:GF-BD	8	75 ± 3	154 ± 1
E70InSi6APP24:GF-BD	24	34 ± 0.1	147 ± 6
E50InSi10APP40:GF-BD	40	20 ± 2	180 ± 9

the absolute flexural modulus values still have inherent uncertainty due to load cell precision. Different load cells with of 1 or 5 kN load with typical precisions of ±0.2% full-scale output, would offer an accuracy of ±2 or ± 10 N, respectively and could be considered in future studies. Similarly, varying the crosshead speed will also be considered to improve accuracy in reporting postfire flexural properties.

4 | Conclusion

In this investigation, a DGEBA resin, cured with DICY and accelerated by Urone was filled with APP FRs and InSi additives at 10%, 30%, and 50% by weight before transfer to GFRCs using prepregs. The GFRCs with a fiber volume content of ~55% were prepared into a facile chocolate-bar inspired structure for fire exposure. A heat flux of 50 kW/m^2 and an exposure time of 5 min were selected for postfire flexural testing, based on visual observations of flame spread across the composite surface. Predictably, the flexural moduli of the composite declined from a range of 5–24 GPa at RT to ~0.1–3 GPa after fire exposure. The prefire flexural strengths of the composites was the strongest indicator of their postfire flexural moduli with an r value of 0.90. In previous work, increasing APP and InSi content was found to enhance char formation, barrier properties, and lower flammability in the composites based on cone calorimetry data. Thus, the formation of loose, unconsolidated char, causes a trade-off effect between fire performance and pre-, in-fire, and postfire mechanics in the composites. The experimental data was compared to calculated values of the postfire flexural modulus via a two-layer and three-region model. A modified two-layer model with an additional interface thickness was found to be more predictive of the postfire flexural modulus in the composites used here due to the undetectability of a partially damaged region in the XCT images necessary within the three-region model. The simplicity of the fire exposure and test method proposed here, can be used as a preliminary basis for the development of a best practice in postfire testing standards. Appropriate safety considerations for the operator during the exposure of the samples were implemented against heat exposure, smoke inhalation, and other risks. In future studies, composites with synergistic FRs will be investigated to determine the reproducibility of the proposed exposure and test method for different fire residues. The ISO 14125 norm was used in this investigation to understand the flexural behavior of the materials. The results of these tests provide a basis for potential industrial applications in cabin interior and compartment materials that retain load-bearing capacity after fire exposure in construction, aerospace, automotive, and railway applications. These include cladding, partition walls, load-bearing beams in electric vehicle battery enclosures and fire-resistant panels for interiors and heavy vehicles. Postfire flexural stress and modulus reflect the load-bearing capacity of components subjected to lateral forces or uneven loads, and resistance to thermal softening, matrix degradation, and fiber-matrix delamination—common failure mechanisms in fire. While flexural testing remains simple and practical for assessing mechanical performance under fire conditions, additional tests (e.g., tensile or shear) may provide a more comprehensive understanding of postfire mechanical behavior. Future investigations could focus on experimental models or simulations to deepen the understanding of these relationships.

Acknowledgments

The authors would like to thank the German Research Foundation (DFG) with the grant number AL 474/53-1 and DFG SCHA 730/26-1 for funding the project and Prof. Dr.-Ing. Volker Altstädt for his contribution to the project. The authors thank Alexandra Krasmik for the contribution to preparing the chocolate-bar inspired structures. The authors thank Keylab of the Bavarian Polymer Institute and Annika Pfaffenberger for contribution to the SEM measurements. The authors would like to thank Christian Bauer, Ute Kuhn, and Andreas Mainz for assistance with sample preparation and testing. Open Access funding enabled and organized by Projekt DEAL.

Conflicts of Interest

The authors declare no conflicts of interest.

Data Availability Statement

The data from this investigation is available from the authors upon reasonable request.

References

1. M. L. Cain, *Epoxy Resins: Synthesis Applications and Recent Developments* (New York: Nova Science Publishers Incorporated, 2016).

2. P. K. Mallick, "Materials, Manufacturing, and Design," *Mechanical Engineering (Marcel Dekker Inc.)* 83 (2007): 74–81.

3. R. F. Gibson, *Principles of Composite Material Mechanics* (Boca Raton, FL: CRC Press, 2007), https://www.taylorfrancis.com/books/mono/10.1201/9781420014242/principles-composite-material-mechanics-ronald-gibson.

4. A. K. Kaw, *Mechanics of Composite Materials* (Boca Raton, FL: CRC Press, 2005), https://www.taylorfrancis.com/books/mono/10.1201/9781420058291/mechanics-composite-materials-autar-kaw.

5. B. K. Kandola, F. Magnoni, and J. R. Ebdon, "Flame Retardants for Epoxy Resins: Application-Related Challenges and Solutions," *Vinyl Additive Technology* 28, no. 1 (2022): 17–49, https://doi.org/10.1002/vnl.21890.

6. F. J. Martin and K. R. Price, "Flammability of Epoxy Resins," *Journal of Applied Polymer Science* 12, no. 1 (1968): 143–158, https://doi.org/10.1002/app.1968.070120114.

7. H. Vahabi, M. R. Saeb, and G. Malucelli, *Analysis of Flame Retardancy in Polymer Science* (Amsterdam, the Netherlands: Elsevier, 2022).

8. B. Schartel, C. A. Wilkie, and G. Camino, "Recommendations on the Scientific Approach to Polymer Flame Retardancy: Part 1—Scientific Terms and Methods," *Journal of Fire Sciences* 34, no. 6 (2016): 447–467, https://doi.org/10.1177/0734904116675881.

9. P. Khalili, K. Y. Tshai, D. Hui, and I. Kong, "Synergistic of Ammonium Polyphosphate and Alumina Trihydrate as Fire Retardants for Natural Fiber Reinforced Epoxy Composite," *Composites Part B: Engineering* 114 (2017): 101–110, https://doi.org/10.1016/j.compositesb.2017.01.049.

10. L. Zhong, K. X. Zhang, X. Wang, M. J. Chen, F. Xin, and Z. G. Liu, "Synergistic Effects and Flame-Retardant Mechanism of Aluminum Diethyl Phosphinate in Combination With Melamine Polyphosphate and Aluminum Oxide in Epoxy Resin," *Journal of Thermal Analysis and Calorimetry* 134, no. 3 (2018): 1637–1646, https://doi.org/10.1007/s10973-018-7699-4.

11. G. M. Wu, B. Schartel, M. Kleemeier, and A. Hartwig, "Flammability of Layered Silicate Epoxy Nanocomposites Combined With Low-Melting Inorganic Ceepree Glass," *Polymer Engineering and Science* 52, no. 3 (2012): 507–517, https://doi.org/10.1002/pen.22111.

12. W. Liu, Y. T. Pan, J. Zhang, et al., "Low-Melting Phosphate Glasses as Flame-Retardant Synergists to Epoxy: Barrier Effects vs Flame Retardancy," *Polymer Degradation and Stability* 185 (2021): 109495.

13. C. H. Ke, J. Li, K. Y. Fang, et al., "Synergistic Effect Between a Novel Hyperbranched Charring Agent and Ammonium Polyphosphate on the Flame Retardant and Anti-Dripping Properties of Polylactide," *Polymer Degradation and Stability* 95, no. 5 (2010): 763–770, https://doi.org/10.1016/j.polymdegradstab.2010.02.011.

14. W. P. Lim, M. Mariatti, W. S. Chow, and K. T. Mar, "Effect of Intumescent Ammonium Polyphosphate (APP) and Melamine Cyanurate (MC) on the Properties of Epoxy/Glass Fiber Composites," *Composites Part B: Engineering* 43, no. 2 (2012): 124–128.

15. M. Rajaei, N. K. Kim, S. Bickerton, and D. Bhattacharyya, "A Comparative Study on Effects of Natural and Synthesised Nano-Clays on the Fire and Mechanical Properties of Epoxy Composites," *Composites Part B: Engineering* 165 (2019): 65–74, https://doi.org/10.1016/j.compositesb.2018.11.089.

16. S. Sunder, M. Jauregui Rozo, S. Inasu, B. Schartel, and H. Ruckdäschel, "A Systematic Investigation of the Transfer of Polyphosphate/Inorganic Silicate Flame Retardants From Epoxy Resins to Layered Glass Fiber-Reinforced Composites and Their Post-Furnace Flexural Properties," *Polymer Composites* 45 (2024): 9389–9406, https://doi.org/10.1002/pc.28416.

17. M. J. Rozo, S. Sunder, H. Ruckdäschel, and B. Schartel, "Char, Gas, and Action: Transfer of the Flame-Retardant Modes of Action in Epoxy Resins and Their Fiber-Reinforced Composites," *Polymer Testing* 140 (2024): 108610, https://doi.org/10.1016/j.polymertesting.2024.108610.

18. T. M. Vetter, J. Bibinger, F. Zimmer, S. Eibl, and H. J. Gudladt, "Characterization of One-Sided Thermal Damage of Carbon Fiber Reinforced Polymers by Means of Depth Profiles," *Journal of Composite Materials* 54, no. 24 (2020): 3699–3713, https://doi.org/10.1177/0021998320917190.

19. J. Bibinger, S. Eibl, and H. J. Gudladt, "Ply-Resolved Quantification of Thermal Degradation in Carbon Fibre-Reinforced Polymers," *Journal of Composite Materials* 57, no. 6 (2023): 1057–1072, https://doi.org/10.1177/00219983221150048.

20. A. P. Mouritz, "Post-Fire Flexural Properties of Fibre-Reinforced Polyester, Epoxy and Phenolic Composites," *Journal of Materials Science* 37, no. 7 (2002): 1377–1386, https://doi.org/10.1023/A:1014520628915.

21. J. Bibinger, S. Eibl, and H. J. Gudladt, "Influence of Low and Extreme Heat Fluxes on Thermal Degradation of Carbon Fibre-Reinforced Polymers," *Applied Composite Materials* 29, no. 5 (2022): 1817–1840, https://doi.org/10.1007/s10443-022-10043-2.

22. E. Toubia, A. Morgan, and A. Elmushyakhi, "Post-Fire Residual Mechanical Properties of a Composite Laminate—Experimental Study," (Boca Raton, FL: CAMX- The Composites and Advanced Materials Expo, 2017), 11–14.

23. J. Zhuge, J. Gou, R. H. Chen, and J. Kapat, "Finite Difference Analysis of Thermal Response and Post-Fire Flexural Degradation of Glass Fiber Reinforced Composites Coated With Carbon Nanofiber Based Nanopapers," *Composites Part A: Applied Science and Manufacturing* 43, no. 12 (2012): 2278–2288.

24. V. Benoit, L. Cédric, and C. Alexis, "Post Fire Behavior of Carbon Fibers Polyphenylene Sulfide- and Epoxy-Based Laminates for Aeronautical Applications: A Comparative Study," *Materials and Design* 63 (2014): 56–68, https://doi.org/10.1016/j.matdes.2014.05.046.

25. M. A. Maaroufi, Y. Carpier, B. Vieille, L. Gilles, A. Coppalle, and F. Barbe, "Post-Fire Compressive Behaviour of Carbon Fibers Woven-Ply Polyphenylene Sulfide Laminates for Aeronautical Applications," *Composites Part B: Engineering* 119 (2017): 101–113.

26. Y. Bai and T. Keller, "Modeling of Post-Fire Stiffness of E-Glass Fiber-Reinforced Polyester Composites," *Composites Part A: Applied Science and Manufacturing* 38, no. 10 (2007): 2142–2153.

27. B. Vieille, A. Coppalle, Y. Carpier, M. A. Maaroufi, and F. Barbe, "Influence of Matrix Nature on the Post-Fire Mechanical Behaviour of Notched Polymer-Based Composite Structures for High Temperature Applications," *Composites Part B: Engineering* 100 (2016): 114–124.

28. C. Katsoulis, B. K. Kandola, P. Myler, and E. Kandare, "Post-Fire Flexural Performance of Epoxy-Nanocomposite Matrix Glass Fibre Composites Containing Conventional Flame Retardants," *Composites. Part A, Applied Science and Manufacturing* 43, no. 8 (2012): 1389–1399, https://doi.org/10.1016/j.compositesa.2012.03.009.

29. N. Kim and D. Bhattacharyya, "Fire Reaction and Post-Fire Impact Properties of Flax Fibre Reinforced Composites Containing Intumescent Flame Retardants," *Journal of Reinforced Plastics and Composites* 43, no. 1–2 (2024): 111–126, https://doi.org/10.1177/07316844231158112.

30. C. Zhu, S. Li, J. Li, et al., "Fire Performance of Sandwich Composites With Intumescent Mat Protection: Evolving Thermal Insulation, Post-Fire Performance and Rail Industry Testing," *Fire Safety Journal* 116 (2020): 103205.

31. E. Kandare, B. K. Kandola, and P. Myler, "Evaluating the Influence of Varied Fire-Retardant Surface Coatings on Post-Heat Flexural Properties of Glass/Epoxy Composites," *Fire Safety Journal* 58 (2013): 112–120, https://doi.org/10.1016/j.firesaf.2013.01.009.

32. T. J. Aspinall, E. L. Erskine, D. C. Taylor, and R. M. Hadden, "Effect of Fibre Orientation and Thermal Exposure on the Post-Fire Mechanical Behaviour of Carbon Fibre Reinforced Polymer Material," *Fire and Materials* 48, no. 1 (2024): 16–38, https://doi.org/10.1002/fam.3163.

33. H. Li, E. Kandare, S. Li, et al., "Integrated Thermal, Micro-and Macro-Mechanical Modelling of Post-Fire Flexural Behaviour of Flame-Retarded Glass/Epoxy Composites," *Computational Materials Science* 59 (2012): 22–32.

34. A. P. Mouritz, C. P. Gardiner, Z. Mathys, and C. R. Townsend, "Post-Fire Properties of Composites Burnt by Cone Calorimetry and Large-Scale Fire Testing," in *ICCM13, International Committee on Composite Materials* (Beijing, China: 2001), 1273.

35. M. D. Gilbert, "Mechanism and Kinetics of the Dicyandiamide Cure of Epoxy Resins" (Doctoral diss., University of Massachusets, Amherst, 1896–February 2014, 1988), https://doi.org/10.7275/3w7s-4d76.

36. M. Hayaty, H. Honarkar, and M. H. Beheshty, "Curing Behavior of Dicyandiamide/Epoxy Resin System Using Different Accelerators," *Iranian Polymer Journal* 22 (2013): 591–598.

37. S. Sunder, M. Jauregui Rozo, S. Inasu, B. Schartel, and H. Ruckdäschel, "Investigating the Changing Dynamics of Processing, Temperature-Based Mechanics, and Flame Retardancy in the Transfer of Ammonium Polyphosphate/Inorganic Silicate Flame Retardants From Epoxy Resins to Glass Fiber Composites," *Journal of Applied Polymer Science* 141, no. 39 (2024): e55988, https://doi.org/10.1002/app.55988.

38. T. W. Loh, E. Kandare, and K. T. Q. Nguyen, "The Effect of Thickness on the Compression Failure of Composite Laminates in Fire," *Composite Structures* 286 (2022): 115334, https://doi.org/10.1016/j.compstruct.2022.115334.

39. W. Tabaka, S. Timme, T. Lauterbach, et al., "Bench-Scale Fire Stability Testing—Assessment of Protective Systems on Carbon Fibre Reinforced Polymer Composites," *Polymer Testing* 102 (2021): 107340, https://doi.org/10.1016/j.polymertesting.2021.107340.

40. B. Schartel, J. K. Humphrey, A. G. Gibson, A. Hörold, V. Trappe, and V. Gettwert, "Assessing the Structural Integrity of Carbon-Fibre Sandwich Panels in Fire: Bench-Scale Approach," *Composites Part B: Engineering* 164 (2019): 82–89, https://doi.org/10.1016/j.compositesb.2018.11.077.

41. W. Tabaka, D. Meinel, and B. Schartel, "Sacrifice Few to Save Many: Fire Protective Interlayers in Carbon-Fiber-Reinforced Laminates," *ACS Omega* 9, no. 22 (2024): 23703–23712, https://doi.org/10.1021/acsomega.4c01408.

42. B. Lattimer and T. Campbell, "Fire Modelling of Composites," in *Fire Properties of Polymer Composite Materials. Solid Mechanics and Its Applications*, vol. 143 (Netherlands: Springer, 2006), 103–132, https://doi.org/10.1007/978-1-4020-5356-6_4.

43. S. V. Levchik and E. D. Weil, "Thermal Decomposition, Combustion and Flame-Retardancy of Epoxy Resins—A Review of the Recent Literature," *Polymer International* 53, no. 12 (2004): 1901–1929, https://doi.org/10.1002/pi.1473.

44. G. Camino and L. Costa, "Performance and Mechanisms of Fire Retardants in Polymers—A Review," *Polymer Degradation and Stability* 20, no. 3–4 (1988): 271–294.

45. C. Thiyagu and U. NarendraKumar, "Effect of Ammonium Polyphosphate on Fire-Retardant, Mechanical, and Vibrational Analysis of Epoxy/Glass/Ramie Hybrid Composite," *Polymer Composites* 44, no. 1 (2023): 621–631, https://doi.org/10.1002/pc.27123.

46. F. A. Gonçalves, M. Santos, T. Cernadas, P. Alves, and P. Ferreira, "Influence of Fillers on Epoxy Resins Properties: A Review," *Journal of Materials Science* 57, no. 32 (2022): 15183–15212.

47. R. F. Landel and L. E. Nielsen, *Mechanical Properties of Polymers and Composites* (Boca Raton, FL: CRC Press, 1993).

48. G. Wypych, *Functional Fillers: Chemical Composition, Morphology, Performance, Applications* (Amsterdam, the Netherlands: Elsevier, 2023).

49. R. Riahipour, M. S. Nemati, M. Zadehmohamad, M. R. Abadyan, M. Tehrani, and M. Baniassadi, "Mechanical Properties of an Epoxy-Based Coating Reinforced With Silica Aerogel and Ammonium Polyphosphate Additives," *Polymers and Polymer Composites* 30 (2022): 09673911211069019, https://doi.org/10.1177/09673911211069019.

50. N. K. Chandramohan, "Variation in Compressive and Flexural Strength of the Carbon Epoxy Composites With the Addition of Various Fillers to the Epoxy Resin," *Materials Today Proceedings* 21 (2020): 643–647.

51. A. Somaiah, B. Anjaneya Prasad, and N. N. Kishore, "A Comprehensive Review: Characterization of Glass Fiber Reinforced Polymer Composites With Fillers From a Thermo-Mechanical Perspective," *Materials Today Proceedings* 62 (2022): 3226–3232, https://doi.org/10.1016/j.matpr.2022.04.219.

52. D. H. Vardhan, A. Ramesh, and B. C. M. Reddy, "Effect of Ceramic Fillers on Flexural Strength of the GFRP Composite Material," *Materials Today Proceedings* 37 (2021): 1739–1742.

53. A. Kelly, *Concise Encyclopedia of Composite Materials* (Amsterdam, the Netherlands: Elsevier, 2012).

54. M. Balasubramanian, *Composite Materials and Processing*, vol. 711 (Boca Raton, FL: CRC Press, 2014), https://api.taylorfrancis.com/content/books/mono/download?identifierName=doi&identifierValue=10.1201/b15551&type=googlepdf.

55. M. Rajaei, D. Y. Wang, and D. Bhattacharyya, "Combined Effects of Ammonium Polyphosphate and Talc on the Fire and Mechanical Properties of Epoxy/Glass Fabric Composites," *Composites Part B: Engineering* 113 (2017): 381–390, https://doi.org/10.1016/j.compositesb.2017.01.039.

56. W. D. Callister and D. G. Rethwisch, *Materials Science and Engineering: An Introduction* (New York, NY: Wiley, 1999), http://sutlib2.sut.ac.th/sut_contents/H100191.pdf.

57. A. A. Stec and T. R. Hull, "17 Fire Toxicity and Its Assessment," in *Fire Retardancy of Polymeric Materials* (Boca Raton, FL: CRC Press, 2009), 453.

58. U. Sorathia, C. Beck, and T. Dapp, "Residual Strength of Composites During and After Fire Exposure," *Journal of Fire Sciences* 11, no. 3 (1993): 255–270, https://doi.org/10.1177/073490419301100305.

59. A. P. Mouritz and A. G. Gibson, *Fire Properties of Polymer Composite Materials* (Berlin, Germany: Springer Science & Business Media, 2007).

Supporting Information

Additional supporting information can be found online in the Supporting Information section.